

Investigating the In-Flight Performance of the UVIT Payload on *AstroSat*

P. T. Rahna,^{1*} Jayant Murthy,^{2†} M. Safonova,³ F. Sutaria,² S. B. Gudennavar¹ and S. G. Bubbly¹

¹*Department of Physics and Electronics, CHRIST (Deemed to be University), Bengaluru 560029, India*

²*Indian Institute of Astrophysics, Bengaluru 560034, India*

³*M. P. Birla Institute of Fundamental Research, Bengaluru 560001, India*

Accepted . Received ; in original form

ABSTRACT

We have studied the performance of the Ultraviolet Imaging Telescope payload on *AstroSat* and derived a calibration of the FUV and NUV instruments on board. We find that the sensitivity of both the FUV and NUV channels is as expected from ground calibrations, with the FUV effective area about 35% and the NUV effective area about the same as that of *GALEX*. The point spread function of the instrument is on the order of 1.2 – 1.6". We have found that pixel-to-pixel variations in the sensitivity are less than 10% with spacecraft motion compensating for most of the flat-field variations. We derived a distortion correction but recommend that it be applied post-processing as part of an astrometric solution.

Key words: instrumentation: detectors, techniques: photometric, ultraviolet: general

1 INTRODUCTION

The *AstroSat* satellite was launched by the Indian Space Research Organization (ISRO) on Sept. 28, 2015 into a near-equatorial (inclination 6°) orbit with an altitude of 650 km (Singh et al. 2014). One of the instruments aboard the satellite is the Ultraviolet Imaging Telescope (UVIT) designed to observe large areas of the sky (field of view: 28' diameter) with a resolution better than 1.8" (Kumar et al. 2012). UVIT was built by the Indian Institute of Astrophysics (IIA) in collaboration with the Inter-University Centre for Astronomy and Astrophysics (IUCAA), the Canadian Space Agency (CSA) and ISRO. It consists of two co-aligned telescopes with three identical intensified CMOS detectors in the far-ultraviolet (FUV), near-ultraviolet (NUV) and visible (VIS).

The ground calibration of the UVIT has been discussed by Postma et al. (2011), and the in-flight tests by Subramaniam et al. (2016). The in-flight calibration of the instrument has been presented by Tandon et al. (2017a). In this work, we present an independent evaluation of the performance of the UVIT FUV and NUV detectors based on observations taken in the Performance and Verification (PV) phase with additional data from our own observations and later calibration observations. The VIS channel was intended only for tracking purposes and its characteristics will have to be

investigated in detail in order to use it for scientific purposes. We will defer this to a further work. The data were reduced and analysed using the *JUDE* (Jayant's UVIT Data Explorer: Murthy et al. (2016); Murthy et al. (2017)) software. Because we have used an independent software system and different calibration techniques, this work provides a verification of the UVIT processing software and the calibration.

2 SPACECRAFT AND UVIT INSTRUMENT

AstroSat was conceived as India's first dedicated astronomy satellite with three X-ray instruments and a UV payload (UVIT) (Pati & Rao 1998; Pati 1999). A recent overview of the *AstroSat* satellite and its mission was presented by Singh et al. (2014) with a description of the flight configuration of UVIT in Tandon et al. (2017b). The various payloads on *AstroSat* were turned on in sequence after the launch, with UVIT being the last payload to begin observing on November 30, 2015 with an observation of the open cluster NGC 188.

UVIT consists of two identical Ritchey-Chrétien telescopes with intensified CMOS detectors: one telescope with a CsI detector (FUV channel) with the other telescope feeding two detectors through a dichroic. The dichroic reflects light in the NUV spectral range onto a CsTe photocathode and transmits the visible light onto an S20 photocathode. Each channel is equipped with a filter wheel with 5 filters providing spectral coverage in a number of passbands from

* E-mail: 7rehanrenzin@gmail.com

† E-mail: jmurthy@yahoo.com

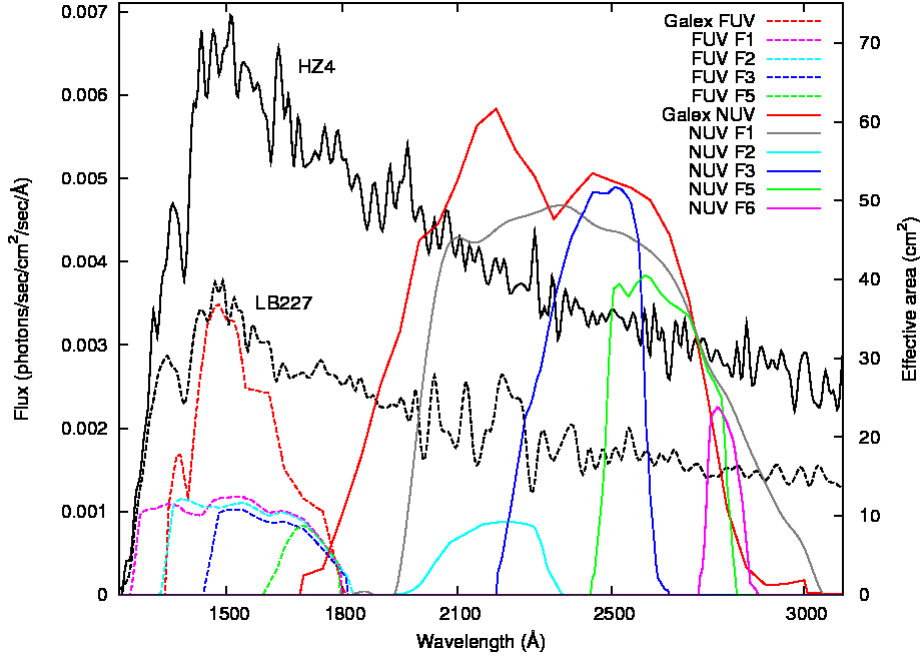


Figure 1. Plots of standard stars spectra with over plotted effective areas of UVIT and *GALEX* filters.

Table 1. General properties of UVIT filters

Filter Channel	Slot (F)	Type	Passband (nm)	Effective bandwidth $\Delta\lambda$ (nm)	Central λ_0 (nm)
FUV	0	Block			
	1	CaF ₂ -1	125 – 179	44.1	150.94
	2	BaF ₂	133 – 183	37.8	154.96
	3	Sapphire	145 – 181	27.4	160.7
	5	Silica	160 – 179	13.13	170.3
NUV	7	CaF ₂ -2	126 – 179	42	151.7
	0	Block			
	1	Silica	194 – 304	76.9	241.8
	2	NUV15	190 – 240	27.1	218.5
	3	NUV13	220 – 265	28.17	243.6
VIS	5	NUVB4	245 – 282	28.23	262.8
	6	NUVN2	273 – 288	8.95	279.0
	0	Block			
	1	VIS3	385 – 530	107.65	458.6
	2	VIS2	360 – 410	36.24	390.5
	3	VIS1	318 – 374	37.65	347.4
	4	Neutral Density	366 – 533	97.0	450.1
	5	BK7 Window	304 – 550	185.	430.7

the FUV to the visible (Table 1). The effective bandwidth in Table 1 is the integral of the normalized effective area, with the central (or ‘mean’) source-independent wavelength defined as

$$\lambda_0 = \frac{\int \lambda A_{\text{norm}}(\lambda) d\lambda}{\int A_{\text{norm}}(\lambda) d\lambda}, \quad (1)$$

where A_{norm} is the effective area normalized to 1. We have plotted the effective areas measured during the ground calibrations (available at <http://uvit.iiap.res.in/Instrument/Filters>) in Fig. 1.

3 CALIBRATION

3.1 Overview

The UVIT instrument was calibrated in the M. G. K. Menon Space Science Laboratory at the Indian Institute of Astrophysics with results described by Kumar et al. (2012). The first 6 months of the mission were dedicated to the performance and verification (PV) phase when selected targets were viewed through different filter combinations. These observations and their analysis and reduction have been discussed by Subramaniam et al. (2016) and Tandon et al. (2017b). We have used these observations along with our own Guaranteed Time (GT) and AO observations to independently characterize the in-flight performance of the

UVIT instrument. All our observations begin with the Level 1 data created by the Indian Space Science Data Centre (ISSDC). We have processed these data through the *JUDE* software (Murthy et al. 2016; Murthy et al. 2017) to create photon event lists and images of the sky.

3.2 Photometric Calibration

3.2.1 Standard Calibrators

Two standard stars were observed as part of the UVIT calibration program: white dwarfs LB227 and HZ4, both of which are standard calibrators of the instruments on the *Hubble Space Telescope* (Bohlin 1996). We obtained their spectra from the CALSPEC database¹ and smoothed with a natural cubic spline. The spectra of the two stars are plotted in Fig. 1 along with the effective area curves of the UVIT FUV and NUV filters and both *GALEX* bands. The UVIT effective areas are from <http://uvit.iap.res.in/Instrument/Filters> and the *GALEX* effective areas from the SVO Filter Profile Service (Rodrigo et al. 2012). We convolved the stellar spectrum with the effective area curve of each filter and have tabulated the expected count rate in Table 2.

The standard operating procedure for the FUV and NUV detectors is to read the 512×512 full frame at a rate of 29 frames per second; faster readouts (up to 600 per second) with smaller windows are available but we only used full-frame observations here. For the purposes of this work, we have defined an observation as a contiguous set of data frames; i.e. we did not co-add different data sets where, for whatever reason, there was a time gap of more than 10 seconds in the data. With this definition, we have 59 independent observations of HZ4 over 4 orbits, and 22 observations of LB227 in one orbit taken over the period Feb. to Dec. 2016. We measured the count rate in each of the observations and tabulated the weighted mean and standard deviation in Table 2, assuming Poissonian statistics in the observed counts. We compared the observed count rate to that expected from the ground calibration and found that it was between 70% – 90% of the pre-flight values (column ‘Obs./Exp.’ in Table 2). Note that the HZ4 was too bright to observe in most of the NUV filters.

3.2.2 Calibration using *GALEX* data

In principle, the photometric calibration should be done by comparing the observed fluxes to those predicted from the standard stars. However, because only two standard stars were observed in the PV phase (HZ4 and LB227), we have expanded the list to include those stars detected in the FUV and the NUV which were also detected by *GALEX*. The *GALEX* photometric calibration has been described by Morrissey et al. (2007) and was tied to an absolute photometric calibration through observations of hot white dwarfs, including HZ4 and LB227.

We used the IDL (Interactive Data Language²) library routine *find.pro* (adapted from DAOPHOT: Stetson (1987))

¹ <http://www.stsci.edu/hst/observatory/crds/calspec.html>

² <http://www.harrisgeospatial.com/ProductsandTechnology/Software/IDL> led by photon noise and were calculated from the square

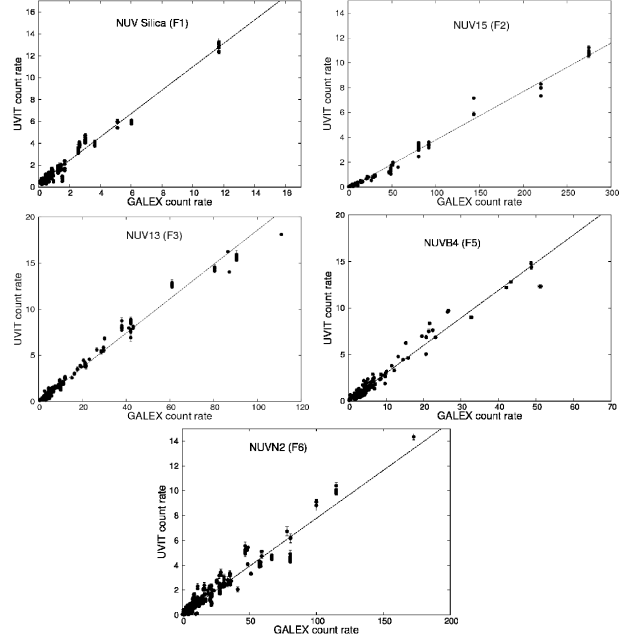


Figure 2. Comparison of UVIT photometry with *GALEX* in different UVIT NUV filters.

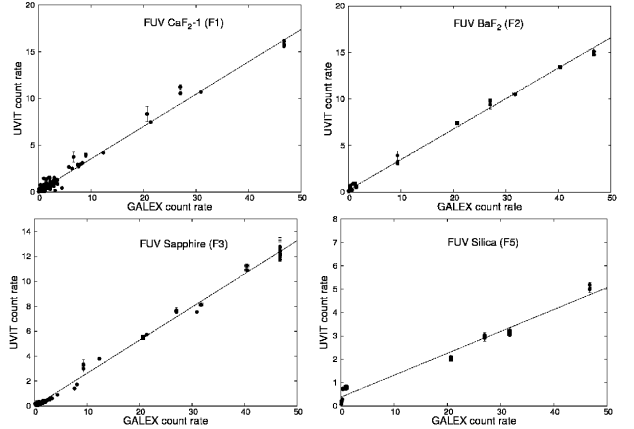


Figure 3. Comparison of UVIT photometry with *GALEX* in different UVIT FUV filters.

to find the point sources in the UVIT images and matched them with *GALEX*. We then used *aper.pro* to perform aperture photometry and extract fluxes from the UVIT images and both *GALEX* bands, where available. If there were multiple *GALEX* observations of a field, we used the one with the greatest exposure time. In each case, we inspected the image to ensure that we were selecting the same source in both UVIT and *GALEX*. Stars used in our calibration are listed in Table 3.

There is a tight correlation between the observed UVIT counts (in all bands) and the *GALEX* counts up to an observed count rate of 15 cps in UVIT above which non-linearity sets in (about 9.7% roll-off, as discussed below). There is effectively no non-linearity in the *GALEX* data at these fluxes because of the faster response time of their delay-line anodes. The errors in either data set are dominated by photon noise and were calculated from the square

Table 2. UVIT count rates (counts s⁻¹) for standard stars.

Filter			HZ4 expected		HZ4 observed		Obs./Exp. ^c	LB227 expected		LB227 observed		Obs./Exp. ^c
				Corr. ^a	mean	stdev			Corr. ^a	mean	stdev	
FUV	CaF ₂ -1	F1	28.94	20.59	15.92	0.19	0.77	15.69	14.17	10.96	0.41	0.77
	BaF ₂	F2	26.34	19.6	14.75 ^d	-	0.75	13.74	-	9.85	0.08	0.72
	Sapphire	F3	17.61	15.34	12.13	0.22	0.79	8.95	-	7.60	0.06	0.85
	Silica	F5	6.33	-	5.12	0.13	0.81	3.09	-	2.99	0.06	0.97
	CaF ₂ -2	F6	25.88	19.41	-	-	-	13.97	-	-	-	-
NUV	Silica	F1	133.55	-	<i>b</i>	-	-	68.75	-	-	-	-
	B15	F2	9.92	-	6.88	0.49	0.69	5.13	-	3.54	0.07	0.69
	B13	F3	49.77	-	<i>b</i>	-	-	25.65	19.32	14.34	0.19	0.74
	B4	F5	35.59	-	<i>b</i>	-	-	18.62	15.92	11.31	0.07	0.71
	N2	F6	6.02	-	4.84	0.27	0.80	3.13	-	2.55	0.04	0.82

^aNon-linearity correction applied (see Sec. 3.2.3).^bWindow mode.^cRatio between observed and expected count rates.^dSingle observation.**Table 3.** Photometry of stars used in the calibration. The full table is available in the electronic attachment.

Star ID	RA [deg]	Dec [deg]	<i>GALEX</i> [counts s ⁻¹]	<i>t</i> _{<i>GALEX</i>} [sec]	UVIT [counts s ⁻¹]	<i>t</i> _{UVIT} [sec]	Fliter	Detector
1	11.9652	85.3188	20.664	222	8.347	12.801	F1	FUV
2	62.3706	17.1315	26.998	14807.95	9.89	326.072	F2	FUV
3	58.842	9.7884	46.752	13321.1	15.039	71.248	F2	FUV
4	20.9410	-58.8057	40.404	219	11.257	630.811	F3	FUV
5	62.3706	17.1315	26.998	14807.95	2.968	244.033	F5	FUV
1	10.6417	-9.2020	11.681	28993.15	12.368	297.733	F1	NUV
2	12.0834	85.2239	92.103	222	3.149	255.785	F2	NUV
3	83.5602	21.9034	21.218	167	3.997	548.825	F3	NUV
4	12.951	-27.1692	43.264	224	12.813	1603	F5	NUV
5	256.536	78.624	80.734	1675.05	6.170	48.7494	F6	NUV

root of the total number of counts. We have used the IDL routine *fitxy.pro* which handles errors in both x and y to calculate the slope and the uncertainty between the UVIT and *GALEX* fluxes in each filter. These are tabulated in Table 4 and plotted in Figs. 2 and 3. The two broadband FUV filters (F1: CaF₂ and F2: BaF₂) have a coverage similar to the *GALEX* FUV band with an effective response of about 35% of the *GALEX* FUV response, as expected from the smaller (35-cm) UVIT primary mirror compared to the *GALEX* primary (50 cm). The smaller UVIT mirror is compensated by the loss in responsivity in the *GALEX* dichroic, and the response of the broadband NUV filter (F1: Silica) is close to that of the *GALEX* NUV band.

We have made no assumptions about the spectral type of each star. This is unimportant for the broad-band filters where the filter response curve for both *GALEX* and UVIT are similar but will impact the narrow-band filters where the source might have emission/absorption lines or the filters may have long tails leading to leakage from out of band counts. This is reflected in the scatter seen particularly in the NUVN2 where the count rate is only about 7% that expected in the *GALEX* NUV band.

We have converted the UVIT-*GALEX* slopes into an absolute calibration using the *GALEX* conversion factors of 1.40×10^{-15} and 2.06×10^{-16} erg cm⁻² s⁻¹ Å⁻¹ (cps)⁻¹ in the FUV and NUV, respectively. The *GALEX* calibration assumed the sources to be spectrally flat, regardless of the actual spectral type. This is obviously an approximation, and a correct calibration should include the spectral type of

the source (Ravichandran et al. 2013). The slope was used as a scale factor to calculate the predicted UVIT count rate to estimate the effect of non-linearity. The scale factors are tabulated in Table 4 and include the effects of the smaller bandpass of the narrow-band filters. Note that it is important to consider the spectral shape of the source when calculating the flux, particularly for the narrow-band filters. The flux $F(\lambda)$ can be derived from the counts using the following equation,

$$F(\lambda) = C \times CPS, \quad (2)$$

where the conversion factors C for UVIT for each filter are given in Table 4. These conversion factors (in units of erg cm⁻² Å⁻¹ cnt⁻¹) were derived using the UVIT/*GALEX* slopes (Figs. 2 and 3) as follows

$$C_{\text{UVIT}} = \frac{C_{\text{GALEX}}}{\text{slope}}. \quad (3)$$

3.2.3 Non-linearity

Intensified detectors are subject to non-linearity at high count rates because the detectors can only register one count per pixel per frame (Fordham et al. 2000). We have compared the observed UVIT count rates in both FUV and NUV channels for all filters (Fig. 4) with the scaled count rates (*GALEX* count rate multiplied with slope in Table 4). We have used the formulation of Kuin & Rosen (2008) to model

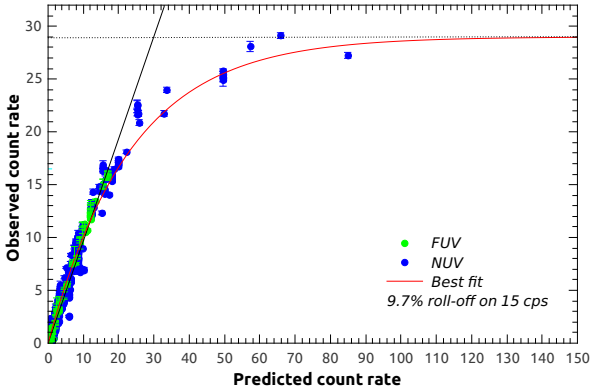


Figure 4. Observed counts as a function of predicted counts for FUV (green points) and NUV (blue points).

the non-linearity:

$$C_{\text{obs}} = 29 \times \left(1 - e^{-\alpha C_{\text{inc}}/29}\right), \quad (4)$$

where $\alpha = 1.24$ (determined empirically), C_{inc} is the number of events incident on the detector, C_{obs} is the number of events detected, and there are 29 frames in a second. Non-linearity in the observed counts sets in at 15 cps with about 9.7% loss and may be corrected for up to 29 cps, at which the measured count rates saturate and the true counts can no longer be recovered.

3.3 Temporal variation in sensitivity

To estimate the possible loss in sensitivity over time, we have compared the counts of stars whose observations were performed over long enough baseline; in three FUV filters and in two NUV filters. We have used two bright stars in NGC 188 cluster (Star 1: BD+8412, star 2: NGC188 2091), in addition to HZ4, and plotted their count rates in Fig. 5. We find no evidence that the sensitivity has changed with time.

3.4 Geometric Distortion

A ground measurement of the geometric distortion is available for the UVIT detectors alone, carried out before integration with the optical assembly (Girish et al. 2017). The measurement was done using a grid of pinholes, the geometric configuration (i.e. pinhole spacing etc.) of which was calibrated using the IUCAA Faint Object Spectrograph & Camera (IFOSC). The geometric distortion of IFOSC itself is only known via simulations. Girish et al. (2017) found a complex distortion pattern and reported the improvement of the astrometry in VIS flight images after applying their distortion correction. This is true, in principle, as one of the limiting factors for the achievable resolution is the spacecraft motion, which is corrected for by applying a shift in x and y . This shift will be affected by the geometric distortion and hence the resolution may not be uniform over the entire detector plane.

Ideally, geometric distortion would have been corrected in-flight through observations of open clusters such as NGC

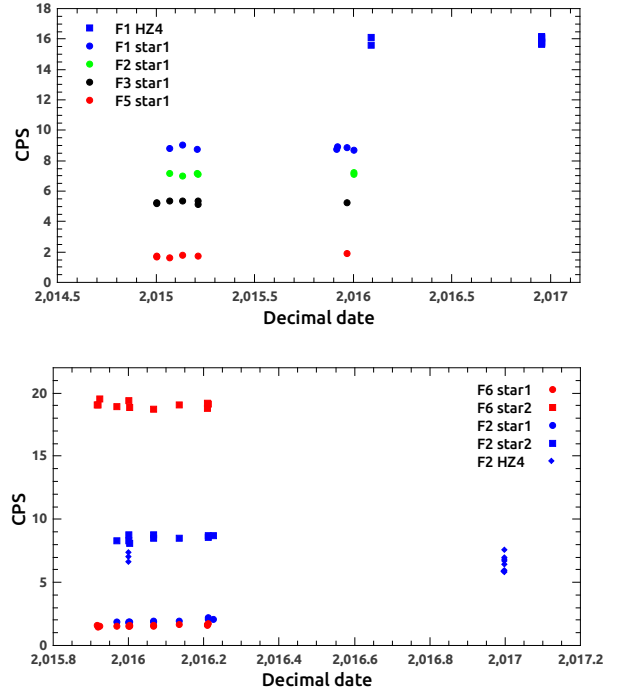


Figure 5. UVIT count rate as a function of date. *Top:* CPS as a function of date of two stars (HZ4 and star 1) in FUV filters. *Bottom:* variation of CPS of HZ4 and star 2 in NUV filters.

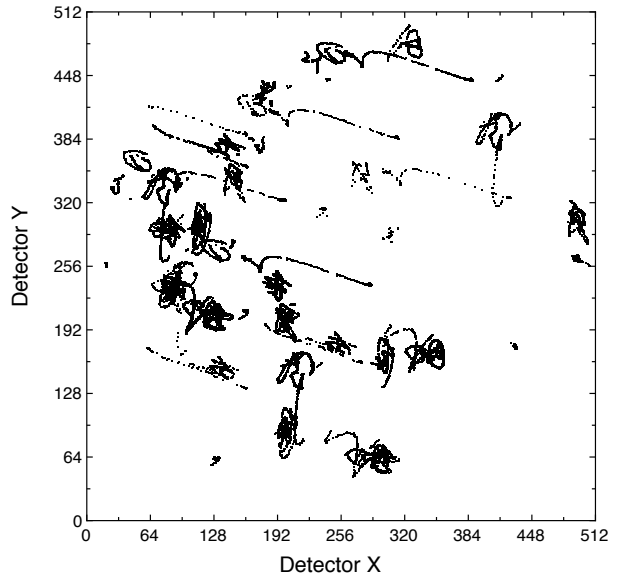


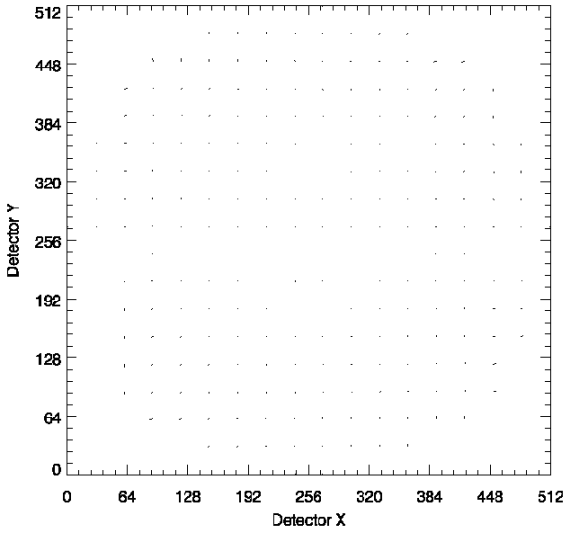
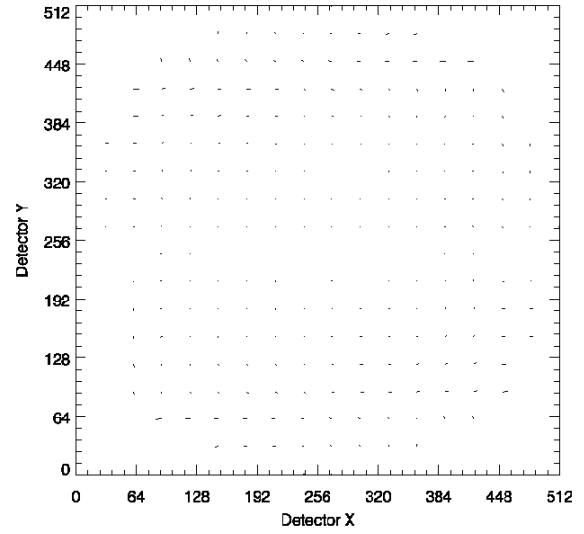
Figure 6. Tracks of individual stars in the detector plane due to spacecraft motion over 9 orbits of NGC 188 in the NUV.

188 but spacecraft motion made it impossible to correlate the positions on the detector plane with the distortion. Instead, we selected three relatively bright stars in the FUV and nine in the NUV observations of NGC 188 and calculated their centroids at intervals of one second. The individual star trails are plotted in Fig. 6 for all NUV observations of NGC 188.

We used the standard SIP (Simple Imaging Polynomial)

Table 4. UVIT conversion factors (in $\text{erg cm}^{-2} \text{ \AA}^{-1} \text{ cnt}^{-1}$).

Filter	Slot	Slope	Slope error (UVIT/GALEX)	R	Conversion factor	Tandon et al. (2017a)	Ratio
FUV CaF2.1	F1	0.3619	0.0013	0.9845	3.8689e-15	3.127E-15	0.81
FUV BaF2	F2	0.3330	0.0018	0.9978	4.2036e-15	3.593E-15	0.85
FUV Sapphire	F3	0.2574	0.0008	0.9986	5.4399e-15	4.402E-15	0.81
FUV Silica	F5	0.0980	0.0011	0.9848	1.4273e-14	1.071E-14	0.75
NUV Silica	F1	1.0586	0.0027	0.9873	1.9459e-16	2.270E-16	1.2
NUV B15	F2	0.0353	0.0001	0.9956	5.8360e-15	5.356E-15	0.91
NUV B13	F3	0.1995	0.0005	0.9941	1.0327e-15	7.412E-16	0.71
NUV B4	F5	0.2959	0.0014	0.9825	6.9611e-16	8.632E-16	1.24
NUV N2	F6	0.0736	0.0002	0.9723	2.7988e-15	3.577E-15	1.28

**Figure 7.** Geometric distortion over the field of view of the NUV detector (full frame).**Figure 8.** Geometric distortion over the field of view of the FUV detector (full frame).

formulation (Shupe et al. 2005)

$$\begin{aligned}
 u &= x + A_{20}(x - 256)^2 + A_{11}(x - 256)(y - 256) \\
 &\quad + A_{02}(y - 256)^2, \\
 v &= y + B_{20}(y - 256)^2 + B_{11}(x - 256)(y - 256) \\
 &\quad + B_{02}(x - 256)^2.
 \end{aligned} \tag{5}$$

to correct the (x, y) pairs in detector coordinates with the centre at $(0, 0)$ into the corrected $u - v$ plane. The angles between stars will remain constant in the undistorted plane, regardless of spacecraft motion, and we determined the coefficients of distortion by forcing the distance between stars in the $u - v$ plane to be the actual angular distance. There is considerable noise in calculating the distortion because of the rapidity of the spacecraft motion and the intrinsic photon noise of the observations in the short time per pixel but we have found a good convergence in the derived coefficients of distortion (Table 5). The distortion maps derived from Eq. 5 for the NUV and FUV detectors are shown in Figs. 7 and 8, respectively.

Although Girish et al. (2017) indicate that applying a distortion correction to the data improves the resolution of the instrument, we find that the effect is small with no mea-

Table 5. Distortion coefficients from Eq. 5 for NUV and FUV channels.

Coefficient	NUV	FUV
A_{20}	-3.7e-05	-4.3e-05
A_{11}	-4.4e-05	-7.1e-05
A_{02}	1.8e-05	1.0e-04
B_{20}	-2.7e-05	-3.4e-05
B_{11}	-6.2e-05	-5.9e-05
B_{02}	2.2e-05	2.8e-05

surable improvement in the instrument PSF. We recommend co-adding the frames in an observation and performing a distortion correction as part of the astrometric solution where the signal-to-noise ratio is better.

3.5 Flat Fielding

The flat field correction accounts for pixel to pixel variations in the sensitivity across the detector but are difficult to determine from in-flight observations because photon counting statistics dominate the signal. We will explore the flat-fielding below but will demonstrate that, in practice, cor-

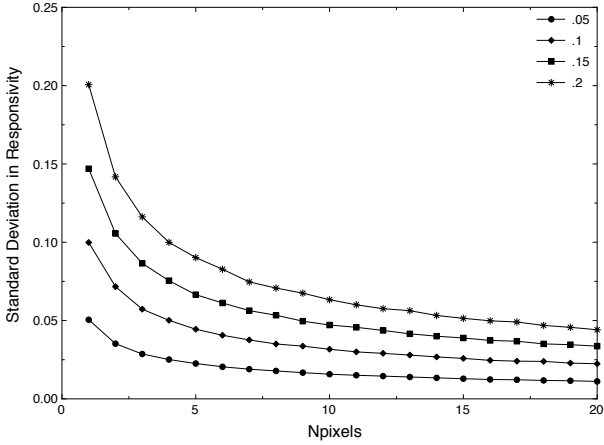


Figure 9. Expected variation in stellar flux due to random fluctuations in pixel sensitivity.

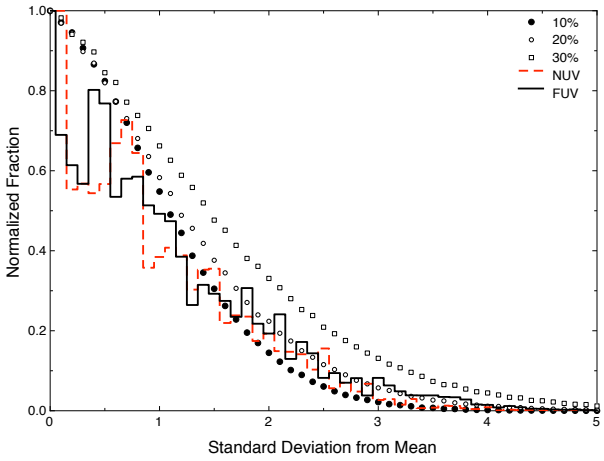


Figure 10. Number of σ away from the mean for the observations (histogram) and different levels of non-uniformity.

rections for the flat-field are unimportant in the context of UVIT because any source is averaged over many pixels due to spacecraft motion.

We have run a number (10,000) of simulations in which we assumed that the point sources were smeared over N pixels, with the sensitivity in each pixel drawn from a normal distribution with a mean of 1 and σ of 5 – 20%. The effective response that any star would see is the mean over the N pixels over which it is smeared and, over a run of 10,000 simulations, will be close to 1. However, the standard deviation will translate into the uncertainty due to the non-uniform sensitivity for stars in different pixels. This is plotted in as a function of N (the number of pixels) in Fig. 9 and suggests that differences of 10% in the sensitivity between pixels would result in an uncertainty of about 2% if the star is smeared over 20 pixels, as is the case for most UVIT observations. We will discuss this in the context of actual observations below.

The most obvious measure of variations in the sensitivity of the detector is the observed count rate for a given source as it moves in the detector plane. We have already tracked the positions of 3 stars in the FUV and 9 in the

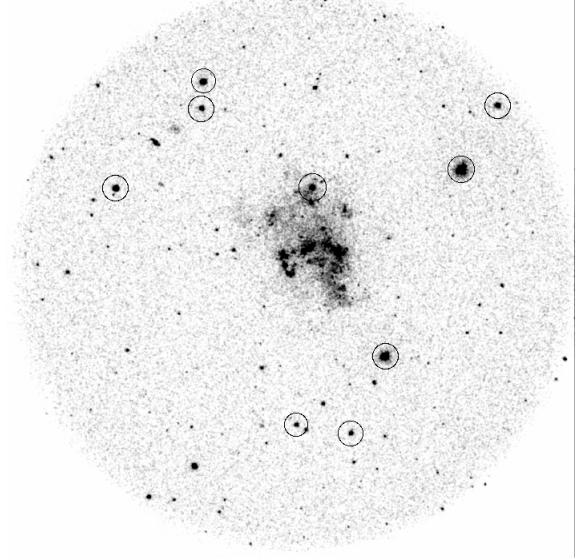


Figure 11. NUV image of Holmberg-II taken on 30 Sept. 2016 with co-added exposure of 1194.6 sec. In black circles are the PSF stars.

NUV observations of NGC 188, and recorded the counts for each pixel in the context of our derivation of the geometric coefficients. These counts will vary because of photon noise and because of the non-uniformity, and we have plotted the deviations from the mean for each pixel in Fig. 10. We then ran a number (10,000) of Monte Carlo simulations where the variation in the count included both photon noise and sensitivity variations of 10%, 20% and 30% per pixel. At this stage in our data analysis, we can only say that the variations in the flat field are less than 10% per pixel, and that it is not necessary to use a flat field in extracting fluxes because of the motion of the spacecraft.

4 PSF

The intrinsic point spread function of the UV detectors is expected to be $1.8''$ (Kumar et al. 2012) but is affected by the spacecraft registration. The primary method of data registration is to use the VIS images in which there are more stars but these have a time resolution of 2.5 seconds during which the spacecraft may move over a significant number of pixels. We have developed a new method (Murthy et al. 2016; Murthy et al. 2017) in which we follow the centroid of a star in the UV images, themselves, in which the time resolution is determined by the brightness of the star but can be as good as 0.35 seconds.

We have used PV observations of NGC 188 and GT observations of Holmberg-II galaxy (e.g. Fig. 11) in which there are a number of stars of different brightness and at least one bright star that we can use to correct for spacecraft motion. We used the *mpfit2dpeak* function in IDL to fit a 2-D Gaussian profile to each of the stellar profiles and calculated the FWHM in both x and y directions. The FWHM is 2.3 pixels ($0.97''$) in the best case, but is more typically in the range from 3 – 4 pixels ($1.2 - 1.6''$). We have found no evidence for any spatial variation of the PSF over the detector plane.

5 CONCLUSIONS

We have performed an independent evaluation of the performance of the UVIT FUV and NUV instruments based on their in-flight performance. We find that the performance is close to that expected from the ground-based calibration. The photometric sensitivity is about 35% that of *GALEX* in the FUV broad band filters and about the same as *GALEX* in the NUV broad band filter. We find that the resolution can be as good as $1.2 - 1.6''$. Flat-fielding is unimportant for UVIT largely because the spacecraft moves enough during an observation that any variations are smeared out. We have derived a distortion correction but since the data are noisy, we recommend that the distortion correction be done as part of the astrometric correction post-processing.

Tandon et al. (2017a) have determined somewhat different calibration factors (Table 4) using only HZ4. This has the advantage that the spectrum of the star is known but is in the non-linear regime in most bands. Those bands with the highest count rates were observed with a high frame rate mode for which the timing was uncertain. We have chosen a broader selection of stars in the linear range of the detectors and tied our calibration to *GALEX* calibration with the assumption that the individual stars will have the same relative response. This appears to be a good approximation given that we obtain excellent correlations between the count rates in both instruments (Figs. 2 and 3) and we believe that, because of the brightness of HZ4, our values better represent the response of the instrument.

Our results serve as a validation of both the UVIT processing software and our alternative set of tools (Murthy et al. 2016). UVIT is beginning to reach its potential and with the opening of the satellite to guest observers, including the international community, we may expect a flood of results in the near future. We will provide support to anyone who would like to use our software, or our results.

ACKNOWLEDGEMENTS

This research has made use of the Spanish Virtual Observatory (SVO) Filter Profile Service (<http://svo2.cab.inta-csic.es/theory/fps/>) supported from the Spanish Ministry of Economy and Competitiveness (MINECO) through grant AyA2014-55216. We also acknowledge the Gnu Data Language (GDL), the Interactive Data Language (IDL) Astronomy Library and its many contributors. This research has made use of National Aeronautics and Space Administration (NASA) Astrophysics Data System Bibliographic Services. Many people at Indian Institute of Astrophysics (IIA), Indian Space Research Organisation (ISRO), Inter-University Centre for Astronomy and Astrophysics (IUCAA), Tata Institute of Fundamental Research (TIFR), National Research Council (NRC, Canada) and University of Calgary have contributed to different parts of the spacecraft, instrument and the operations.

Some/all of the data presented in this paper were obtained from the Mikulski Archive for Space Telescopes (MAST). Space Telescope Science Institute (STScI) is operated by the Association of Universities for Research in Astronomy, Inc., under National Aeronautics and Space

Administration (NASA) contract NAS5-26555. Support for MAST for non-Hubble Space Telescope (HST) data is provided by the NASA Office of Space Science via grant NNX09AF08G and by other grants and contracts.

This research has been supported by the Department of Science and Technology (DST) under grants no. SR/S2/HEP-050/2012 dated 14-08-2013 to Christ University and EMR/2016/00145 to Indian Institute of Astrophysics (IIA).

REFERENCES

- Bohlin R. C., 1996, *Astronom. J.*, **111**, 1743
- Fordham J. L. A., Moorhead C. F., Galbraith R. F., 2000, *Mon. Not. R. Astron. Soc.*, **312**, 83
- Girish V., Tandon S. N., Sriram S., Kumar A., Postma J., 2017, *Experimental Astronomy*, **43**, 59
- Kuin N. P. M., Rosen S. R., 2008, *Mon. Not. R. Astron. Soc.*, **383**, 383
- Kumar A., et al., 2012, in Space Telescopes and Instrumentation 2012: Ultraviolet to Gamma Ray, *Proc. SPIE*. p. 84431N ([arXiv:1208.4670](https://arxiv.org/abs/1208.4670)), doi:10.1117/12.924507
- Morrissey P., et al., 2007, *Astrophys. J. Suppl.*, **173**, 682
- Murthy J., Rahna P. T., Safonova M., Sutaria F., Gudennavar S. B., Bubbly S. G., 2016, JUDE: An Ultraviolet Imaging Telescope pipeline, Astrophysics Source Code Library (ascl:1607.007)
- Murthy J., Rahna P., Sutaria F., Safonova M., Gudennavar S., Bubbly S., 2017, *Astron. Comput.*, **20**, 120
- Pati A. K., 1999, *Bulletin of the Astronomical Society of India.*, **27**, 295
- Pati A. K., Rao N. K., 1998, in Bely P. Y., Breckinridge J. B., eds, *Proc. SPIE* Vol. 3356, Space Telescopes and Instruments V. pp 635–640, doi:10.1117/12.324485
- Postma J., Hutchings J. B., Leahy D., 2011, *Publ. Astr. Soc. Pac.*, **123**, 833
- Ravichandran S., Preethi K., Safonova M., Murthy J., 2013, *Astrophys. Space Sci.*, **344**, 361
- Rodrigo C., Solano E., Bayo A., 2012, SVO Filter Profile Service Version 1.0, IVOA Working Draft 15 October 2012
- Shupe D. L., Moshir M., Li J., Makovoz D., Narron R., Hook R. N., 2005, in Shopbell P., Britton M., Ebert R., eds, *Astronomical Society of the Pacific Conference Series* Vol. 347, *Astronomical Data Analysis Software and Systems XIV*. p. 491
- Singh K. P., et al., 2014, in Space Telescopes and Instrumentation 2014: Ultraviolet to Gamma Ray. *Proc. SPIE*. p. 91441S, doi:10.1117/12.2062667
- Stetson P. B., 1987, *Publ. Astr. Soc. Pac.*, **99**, 191
- Subramaniam A., et al., 2016, in Society of Photo-Optical Instrumentation Engineers (SPIE) Conference Series. p. 99051F ([arXiv:1608.01073](https://arxiv.org/abs/1608.01073)), doi:10.1117/12.2235271
- Tandon S. N., et al., 2017a, preprint, ([arXiv:1705.03715](https://arxiv.org/abs/1705.03715))
- Tandon S. N., et al., 2017b, *Journal of Astrophysics and Astronomy*, **38**, 28